Available online at www.eccomasproceedia.org
Eccomas Proceedia COMPDYN (2021) 3407-3417

ECCOMAS
Proceedia

COMPDYN 2021
8th ECCOMAS Thematic Conference on
Computational Methods in Structural Dynamics and Earthquake Engineering
M. Papadrakakis, M. Fragiadakis (eds.)
Streamed from Athens, Greece, 28 - 30 June 2021

SCOUR-INDUCED DYNAMIC PROPERTIES MODIFICATION OF MASONRY ARCH BRIDGES WITH DIFFERENT GEOMETRY

F. Scozzese[1], L. Ragni[2], E. Tubaldi[3], F. Gara[2]

[1] University of Camerino
Viale della Rimembranza 63100 Ascoli Piceno, Italy
e-mail: fabrizio.scozzese@unicam.it

[2] Università Politecnica delle Marche
Via Brecce Bianche, Ancona (AN), Italy
{laura.ragni, f.gara}@univpm.it

[3] University of Strathclyde
75 Montrose Street, G1 1XQ Glasgow, UK
enrico.tubaldi@strath.ac.uk

Abstract

This paper, focused on the effect of local scour actions on masonry bridges, represents a follow-up of a previous study conducted by the authors aimed at analysing the effect of a localised scour-induced settlement of the pier on the modal properties of the bridge (i.e., frequencies and mode shapes). Results from the previous study showed as the scour phenomenon, even at its early stages could induced a non-negligible variability of the transverse modal shape of a masonry arch bridge selected as case study. In this paper, the work is continued by analysing how the bridge geometry can affect the aforesaid results. To this aim, bridges with three different geometry (130 m length, 100 m length, 50 m length) are analysed by simulating the scour evolution under the piers and by monitoring the modal response at different stages of the excavation. Accurate finite element models are developed in Abaqus, accounting for both mechanical and geometrical nonlinearities.

Keywords: masonry, bridges, scour, Abaqus FEM, arch bridges, modal shapes, OMA.

ISSN:2623-3347
Peer-review under responsibility of the organizing committee of COMPDYN 2021.
doi: 10.7712/120121.8719.18748

1 INTRODUCTION

Scour is a natural phenomenon caused by the erosion or removal of streambed or bank material from bridge foundations due to flowing water [1-3].

This action is among the most common causes of bridge failure worldwide [2-4], leading to notable direct and indirect losses, as witnessed by the numerous cases of scour-induced collapses occurred worldwide [5-8].

Masonry arch bridges are particularly vulnerable to this phenomenon, due to their high stiffness and the usually shallow footings. The relevance of the problem is also witnessed by the increasing number of works dealing with this issue, e.g., numerical studies employing soil-foundation-structure interaction models with different level of complexity [4, 9], works proposing advanced models for describing the cracking mechanism evolution in the masonry components [10-13], and studies oriented towards dynamic identification and scour monitoring [14-17]. Moreover, besides the studies fully dedicated to the seismic response [18, 19], the literature offers an always growing number of papers focused on vulnerability and resilience assessment of masonry bridges under multiple hazard (mainly earthquakes and floods) [20, 21].

In the recent years, studies have been also carried out to investigate the possibility of detecting scour by tracking the changes of the dynamic properties of the bridge-foundation-soil system (see e.g., the studies of [22, 23] in the context of masonry arch bridges, or the ones of [24, 25] for steel and reinforced concrete bridges).

In particular, the study conducted in 2020 by [5] has shown as the scour phenomenon, even at its early stages could induced a non-negligible variability of the transverse modal shape of a masonry arch bridge selected as case study, thus opening the way to mode-shape based scour monitoring techniques. Very recently (in 2021) the work of [26] presented an approach to detect stiffness loss arising due to scour based on relative changes of vertical-pier mode shape amplitudes, by testing the method through a scaled experimental model of a bridge traversed by a vehicle.

Within this framework and as follow-up of [5], the present paper focuses on the effects of a localized scour-induced settlement of the pier on the modal properties (i.e., frequencies and mode shapes) of multi-span masonry arch bridges. In particular, the investigation initiated in [5] is herein extended to bridges with three different geometries: 7-spans 130 m length, 5-spans 100 m length, 3-spans 50 m length. For each of the three bridges an accurate 3D finite element model is first developed in Abaqus [27], accounting for both mechanical and geometrical nonlinearities; then numerical simulations are performed to assess the modal response sensitivity at different stages of the scour process evolution (a single pier is assumed to experience scour).

2 CASE STUDIES

A masonry arch bridge typology very common in the existing Italian infrastructural stock (but also diffused in Europe and worldwide) is considered in this study, and three different geometric schemes are analysed: a 7-spans bridge (131.20 m long), a 5-spans bridge (98.80 m long) and a 3-spans bridge (54.40 m long).

All the bridges have the following features [5, 28] in common: the spans are 16.00 m long; the piers are all identical with a plan size of 9.5 m x 3.2 m, excluding the extreme circular parts with a radius of 2.0 m along the transverse direction (Y direction); the arches have thickness of 0.95 m and a radius of 11.58 m; spandrel walls have thickness of 0.65 m; the pier foundations have a rectangular plan shape of 11.00 m x 3.90 m and their height is 4.15 m. More details about the bridge geometry are given in Figure 1,The longitudinal views of the bridges are provided in Figure 1; two sections (one transversal and one longitudinal) are shown in Figure 2.

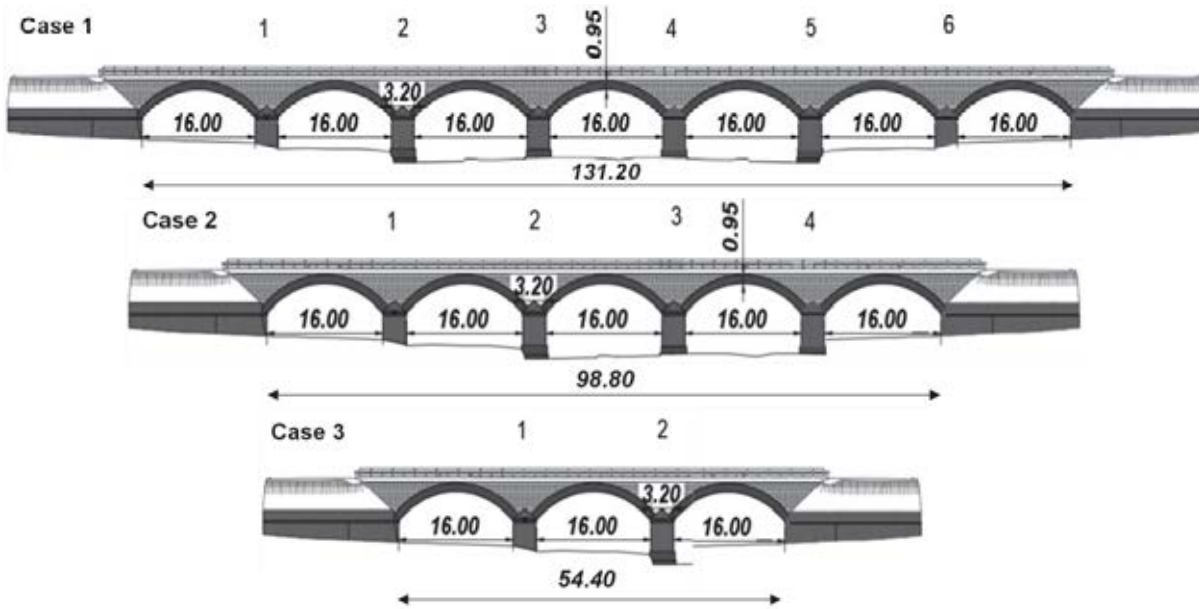

Figure 1. Longitudinal view and geometries of the three case studies.

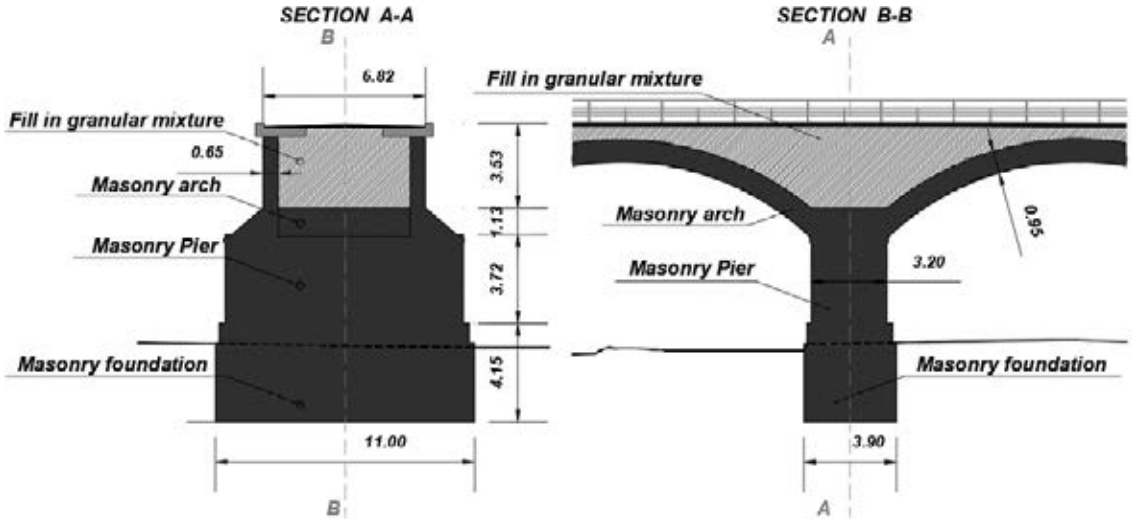

Figure 2. Sections and details common for all the masonry arch bridges.

The materials mechanical properties are taken from [5] and are based on both in-situ and laboratory characterization tests. Table 1 provides a summary of the main mechanical properties of the bridge materials, in terms of density ρ, Young's modulus E, yield stress in compression $f_{y,c}$ (or cohesion c for what concerns the backfill) and peak tensile stress $f_{y,t}$.

Table 1. Material properties.

Material [-]	ρ [t/m^3]	E [kN/m^2]	c - $f_{y,c}$ [kN/m^2]	$f_{y,t}$ [kN/m^2]
Masonry (Arches & Spandrels)	1.80	3100000	2000	150
Masonry (Piers)	1.75	2900000	2000	150
Backfill	1.70	250000	10	0
Abutment	1.90	300000	-	-

Riverbed features are assumed according to the case study analysed in [5], where both geophysical and mechanical soil characterizations were achieved through a set of in-situ tests and laboratory tests. The riverbed properties, made of with highly dense gravel and sands (alluvial deposit extending 27 m below the surface), are collected in Table 2 (friction angle ϕ, Young's modulus E, Poisson's ratio ν, shear modulus G, soil density ρ, and average shear waves velocity v_S).

Table 2. Soil parameters.

ϕ [°]	E [kN/m^2]	ν [–]	G [kN/m^2]	ρ [t/m^3]	v_S [m/s]
38	1065000	0.45	370000	2.0	430

3 MODELLING STRATEGY

3.1 General details of the finite element model and material constitutive laws

A 3D model of each case study (Figure 3) is developed in ABAQUS 2017 [27] by following the strategy adopted in [5] and briefly recalled below.

The bridge model is built by using continuum solid linear hexahedral 8-nodes elements of type C3D8R, with 6 degrees of freedom per node.

A coarser mesh is attributed to master parts in defining contact pairs interaction, in order to avoid penetration at the interface. Moreover, the mesh discretisation is set in order to attain of a good trade-off between results' accuracy and computational effort, with element dimensions varying between 0.35 m and 0.75 m.

The model accounts for both geometrical and mechanical nonlinearities.

The behaviour of the masonry components in the linear elastic field is described by assigning the properties summarised in Table 1. The non-linear behaviour is described through the Concrete Damage Plasticity (CDP) model with the parameters reported in [5].

For the fill material, a linear elastic model is employed, together with a Mohr-Coulomb failure criterion, characterized by a friction angle of 55° and a cohesion of 10 kN/m^2.

As schematically shown in Figure 4, the interaction between the different bridge components is simulated by means of the following nonlinear frictional/cohesive interfaces [4, 5, 10] (see [5] for a detailed discussion of the topic): a frictional interface is used to describe the interaction between the fill and the other bridge components along the tangential direction (the tangential behaviour is characterised by a friction coefficient of 0.60); a "hard-contact" behaviour is assumed along the normal direction, allowing separation but preventing penetration between the parts in contact; cohesive interactions are used for the other interfaces (i.e., spandrel-to-arch, spandrel-to-pier and arch-to-pier), simulating the behaviour of mortar joints between the parts. Moreover, a damage criterion is introduced, whose initiation is governed by the attainment of the maximum nominal stress values along the normal and tangential directions, equal to $f_{n,max}$ = 150 kN/m^2 (Table 1) and $f_{t,max} = 1.4 \cdot f_{n,max}$ = 220 kN/m^2, respectively. The damage evolution is described by the Benzeggagh-Kenane mixed mode fracture criterion, with a power-law exponent of 2.2, and the values of normal and shear fracture energies are assumed equal to $G_{f,n}$ = 0.05 kN/m and $G_{f,s}$ = 0.10 kN/m, respectively. To improve convergence, a damage stabilization criterion is also used, by defining a viscous coefficient of 10^{-5} kNs/m.

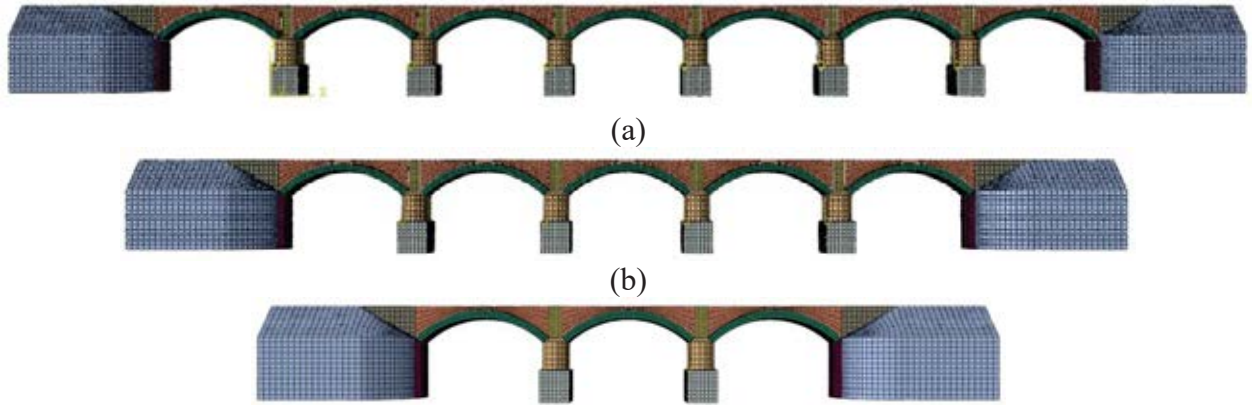

(a) (b) (c)

Figure 3. Finite element models: (a) 7-spans, (b) 5-spans and (c) 3-spans bridge.

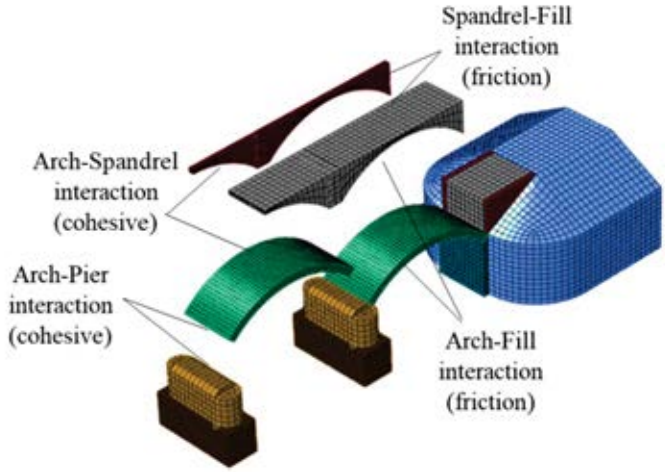

Figure 4. FE model with highlighted materials interface types.

3.2 Scour numerical simulation

A Winkler modelling approach is employed to describe the soil-foundation interaction (Figure 5). The relationship between the soil pressure and the corresponding settlement is described through the following set of equivalent soil stiffness constants (Table 3) $k'_x = \frac{k_x}{A_x}$, $k'_y = \frac{k_y}{A_y}$, $k'_z = \frac{k_z}{A_z}$, with k_x, k_y, k_z (kN/m) provided by Gazetas [29] and A_x, A_y, A_z foundation areas. However, different impedances formulations [30] might also be used.

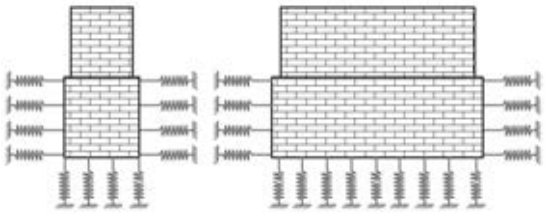

Figure 5. Impedances along the *x*, *y*, *z* directions

Table 3. Soil stiffness constants.

k'_x [kN/m^3]	k'_y [kN/m^3]	k'_z [kN/m^3]
220000	420000	940000

The scour process evolution is numerically modelled according to the simplified procedure proposed in [5], which can be synthetised as follows (Figure 6):

- The hole shape is described by a constant inverted pyramidal form [4].
- The vertex of the pyramid is assumed along a vertical line passing through the centre of the upstream face of the pier, the upstream slope of the hole is taken equal to friction angle at rest of the soil, ϕ, whereas the downstream slope is approximately half that value, consistently with [2].
- The scour hole slope along the direction perpendicular to the flow is equal to $5/6 \cdot \phi$.
- Being the shape of the scour hole fixed, the hole geometry is completely defined by the maximum scour depth y_s, identifying the scour hole vertex, and by the value of the friction angle of the soil.
- A time-history analysis is performed in Abaqus in which, at each time step, the level of the maximum scour depth is increased and the depth of the centroid of each cohesive element representing the foundation-soil interaction is compared with the depth of scour at the same location: if the element centroid is within the scour hole, then the element is deactivated.
- In this study, the simulation of the deepening of the scour hole is described by considering 8 discrete steps.

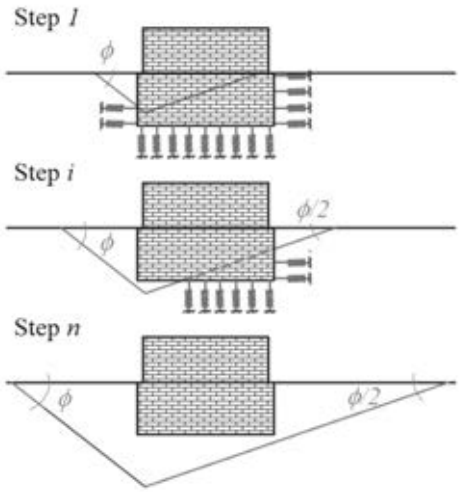

Figure 6. Scheme of scour progression modelling.

Step 0 corresponds to the starting condition, with gravity loads acting on the bridge (self-weight loads plus a uniform pressure of 6.6 kN/m^2 simulating the road pavement loads) and no scour. From Step 1 to Step 7, the scour development is simulated by considering increments of y_s equal to 1.0 m per step, for a total maximum scour depth of 7.0 m attained at Step 7, corresponding to an excavation of 3.0 m under the base of the pier's foundation (whose height is 4.15 m).

At the end of step of analysis, a eigenvalues analysis is performed in order to evaluate the modal shapes and he frequencies of the bridges at the current state (i.e., at the current level of scour). Further details about the simulation and the solver setting are given in [5]. In this study,

the scour is assumed to occur on one single pier only, corresponding to the most extreme one (i.e., near the right abutment).

4 SCOUR INFLUENCE ON BRIDGES DYNAMIC PROPERTIES

In this section the influence of the scour progression on the modal properties of the three bridges is assessed. In particular, for each bridge configuration, the modification of the transversal modal shapes is graphically displayed (Figure 7, Figure 8, Figure 9); it is worth noting that the sequence of mode shapes shown in the figures should be read from the top (no scour taking place) to the bottom (maximum scour excavation).

The variation of the corresponding natural frequencies is reported as well (Table 4 and Table 5): Table 4 illustrates the evolution of the frequency with the scour depth progression, while Table 5 collects the percent variation with respect to the reference value at Step 0.

Despite the different values of the reference frequencies observed by three bridges, a common patter can be found in the results of this investigation. Indeed, the changes of the modal frequency are very low for increasing scour depths between 0.0 m and 4.0 m, with a percentage decrease of 1.5% - 2.44% at Step 4 (i.e., with $y_s = 4.0$ m). From this point on, the effects of the scour on the modal frequency become more and more significant, with percentage reductions higher than 20% at Step 5 (i.e., 1.0 m of excavation under the pier), while very high reductions (>46%) are observed for $y_s = 6.0$ m (i.e., 2.0 m of excavation under the pier).

Table 4. Modal frequency evolution (Hz) at different scour levels.

Bridge	Step 0	Step 1	Step 2	Step 3	Step 4	Step 5	Step 6
	0.0 m	1.0 m	2.0 m	3.0 m	4.0 m	5.0 m	6.0 m
7-spans	6.455	6.453	6.445	6.428	6.357	5.077	3.431
5-spans	6.048	6.045	6.031	6.016	5.952	4.750	3.199
3-spans	6.110	6.101	6.067	6.041	5.961	4.750	3.200

Table 5. Modal frequency percent variation (%) at different scour levels.

Bridge	Step 0	Step 1	Step 2	Step 3	Step 4	Step 5	Step 6
	0.0 m	1.0 m	2.0 m	3.0 m	4.0 m	5.0 m	6.0 m
7-spans	0.00	-0.03	-0.15	-0.42	-1.52	-21.35	-46.85
5-spans	0.00	-0.05	-0.28	-0.53	-1.59	-21.46	-47.11
3-spans	0.00	-0.15	-0.70	-1.13	-2.44	-22.26	-47.63

If from one side the frequency changes remain negligible for a "long time" of scour process evolution, the mode shapes (Figure 7, Figure 8, Figure 9) are found to be more sensitive to the effect of scour. Indeed, a non-negligible variability of the transverse mode shapes is observed on all the three bridges starting from the early stages of the scour phenomenon, i.e., for y_s between 1.5 and 2.0 m, before the stages of excavation under the pier's foundation. As the scour proceeds, the mode shape becomes always more local and interesting the subsiding pier.

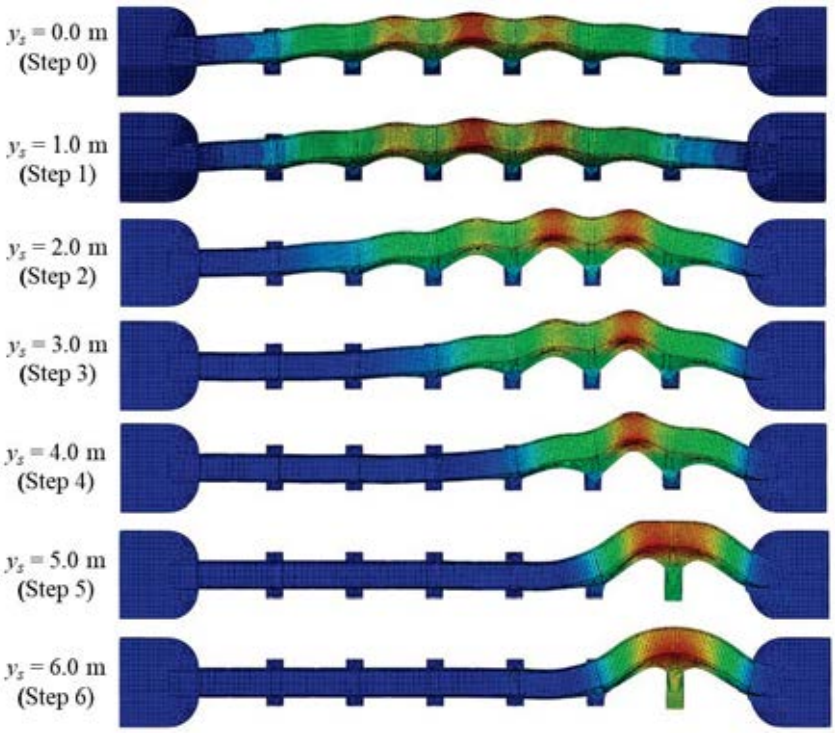

Figure 7. Transverse mode shapes variation for different scour depths.

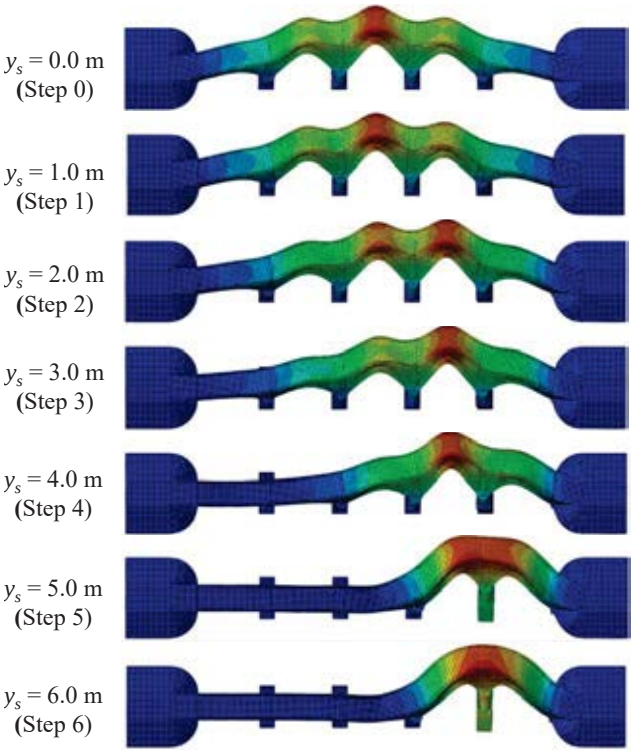

Figure 8. Transverse mode shapes variation for different scour depths.

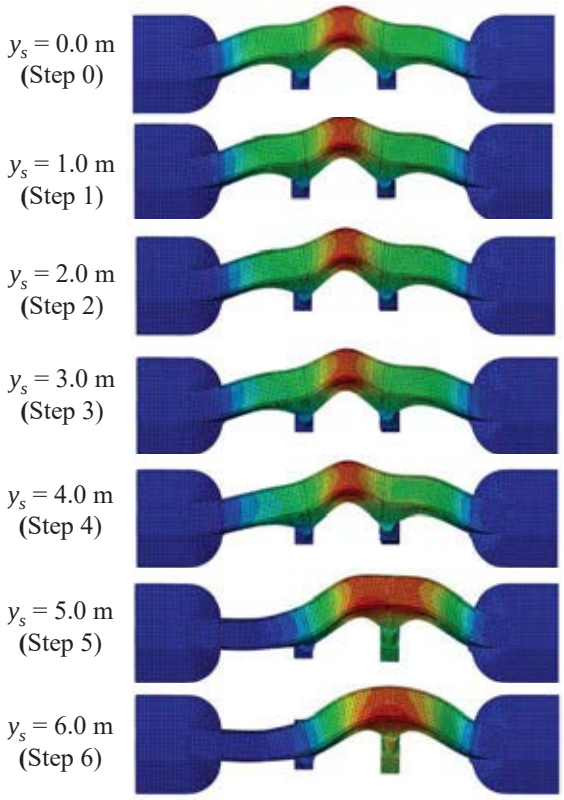

Figure 9. Transverse mode shapes variation for different scour depths.

5 CONCLUSIONS

The effects of a localized scour-induced settlement of the pier on the modal properties (i.e., frequencies and mode shapes) of masonry arch bridges are analysed. As extension of the study of [5], bridges with three different geometries (130 m length, 100 m length, 50 m length) are analysed by simulating the scour evolution under the piers and by monitoring the modal response at different stages of the excavation. Accurate finite element models are developed in Abaqus, accounting for both mechanical and geometrical nonlinearities.

No significative differences are observed among the analysed case studies, characterised by different geometries but equal static scheme, materials and boundary conditions. The results of [5] and the relevant main conclusions thus still hold and can be summarised as follows:

- are negligible if the scour depth involves only the lateral sides of the foundation.
- The modal frequency changes become noticeable (higher than 20%) only when the soil underneath the pier is eroded; for this reason, the suitability of a *frequency-oriented* identification system based on ambient vibrations might be compromised.
- Conversely, the transverse mode shapes exhibit a very high sensitivity to scour, even at the early stages of the phenomenon; in light of this, a *mode shape-oriented* identification system might be appropriate for monitoring the scour evolution over the time and thus intervene timely in order to avoid failure or damage development on masonry bridges.

However, the study shall be extended to a wider set of case studies in order to verify the effectiveness of the proposed OMA-based identification technique as a scour monitoring and early warning strategy in those cases in which scour affects a larger number of piers (scour on a single pier is analysed in this work).

Moreover, un undergoing study is aimed at developing a probabilistic hazard discharge model accounting for the scour refill process due to live-bed flood conditions, based on the recent work [31]. This hazard model will be exploited within a time-dependent risk assessment probabilistic framework for bridges, which may also integrate other source of hazards (e.g., earthquakes [32]).

REFERENCES

[1] Pizarro, A., Manfreda, S., & Tubaldi, E. (2020). The science behind scour at bridge foundations: A review. *Water*, *12*(2), 374.

[2] Hoffmans GJCM, Verheij HJ. Scour Manual. Routledge; 2017. oi:10.1201/9780203740132.

[3] Melville BW, Coleman SE. Bridge scour. Water Resources Publications, LLC; 2000.

[4] Tubaldi E, Macorini L, Izzuddin BA. Three-dimensional mesoscale modelling of multi-span masonry arch bridges subjected to scour. Engineering Structures 2018;165:486–500. doi:10.1016/J.ENGSTRUCT.2018.03.031.

[5] Scozzese, F., Ragni, L., Tubaldi, E., & Gara, F. (2019). Modal properties variation and collapse assessment of masonry arch bridges under scour action. *Engineering Structures*, *199*, 109665.

[6] Sousa JJ, Bastos L. Multi-temporal SAR interferometry reveals acceleration of bridge sinking before collapse. Natural Hazards and Earth System Sciences 2013;13:659–67. doi:10.5194/nhess-13-659-2013.

[7] Gavin K, Obrien EJ. Sustainable Maintenance and Analysis of Rail Transport Infrastructure (SMART rail) Railway bridge safety and condition assessment View project Smart Rail View project. 2012.

[8] Maddison B. Scour failure of bridges. Proceedings of the Institution of Civil Engineers - Forensic Engineering 2012;165:39–52. doi:10.1680/feng.2012.165.1.39.

[9] Zampieri P, Zanini MA, Faleschini F, Hofer L, Pellegrino C. Failure analysis of masonry arch bridges subject to local pier scour. Engineering Failure Analysis 2017;79:371–84. doi:10.1016/J.ENGFAILANAL.2017.05.028.

[10] Zhang Y, Tubaldi E, Macorini L, Izzuddin BA. Mesoscale partitioned modelling of masonry bridges allowing for arch-backfill interaction. Construction and Building Materials 2018;173:820–42. doi:10.1016/J.CONBUILDMAT.2018.03.272.

[11] Milani G, Lourenço PB. 3D non-linear behavior of masonry arch bridges. Computers & Structures 2012;110–111:133–50. doi:10.1016/J.COMPSTRUC.2012.07.008.

[12] Tubaldi, E., Minga, E., Macorini, L., & Izzuddin, B. A. (2020). Mesoscale analysis of multi-span masonry arch bridges. Engineering Structures, 225, 111137.

[13] Rainieri, C., Notarangelo, M. A., & Fabbrocino, G. (2020). Experiences of dynamic identification and monitoring of bridges in serviceability conditions and after hazardous events. Infrastructures, 5(10), 86.

[14] Maroni, A., Tubaldi, E., Ferguson, N., Tarantino, A., McDonald, H., & Zonta, D. (2020). Electromagnetic sensors for underwater scour monitoring. Sensors, 20(15), 4096.

[15] Civera, M., Calamai, G., & Fragonara, L. Z. (2021, April). System identification via Fast Relaxed Vector Fitting for the Structural Health Monitoring of masonry bridges. In Structures (Vol. 30, pp. 277-293). Elsevier.

[16] Wan Mohtar, W. H. M., Muad, A. M., Porhemmat, M., Ab. Hamid, H., & Whayab, S. S. (2021). Measuring scour level based on spatial and temporal image analyses. *Structural Control and Health Monitoring*, *28*(1), e2645.

[17] Lee, M., Yoo, M., Jung, H. S., Kim, K. H., & Lee, I. W. (2020). Study on Dynamic Behavior of Bridge Pier by Impact Load Test Considering Scour. Applied Sciences, 10(19), 6741.

[18] Zampieri, P., Perboni, S., Tetougueni, C. D., & Pellegrino, C. (2020). Different Approaches to Assess the Seismic Capacity of Masonry Bridges by Non-linear Static Analysis. Front. Built Environ, 6, 47.

[19] Gönen, S., & Soyöz, S. (2021). Seismic analysis of a masonry arch bridge using multiple methodologies. Engineering Structures, 226, 111354.

[20] Argyroudis, S. A., Mitoulis, S. A., Hofer, L., Zanini, M. A., Tubaldi, E., & Frangopol, D. M. (2020). Resilience assessment framework for critical infrastructure in a multi-hazard environment: Case study on transport assets. Science of The Total Environment, 714, 136854.

[21] Argyroudis, S. A., & Mitoulis, S. A. (2021). Vulnerability of bridges to individual and multiple hazards-floods and earthquakes. Reliability Engineering & System Safety, 107564.

[22] Ruocci G. Application of the SHM methodologies to the protection of masonry arch bridges from scour. PhD Thesis, Polytechnic University of Torino, 2010.

[23] Foti S, Sabia D. Influence of Foundation Scour on the Dynamic Response of an Existing Bridge. Journal of Bridge Engineering 2011;16:295–304. doi:10.1061/(ASCE)BE.1943-5592.0000146.

[24] Ju SH. Determination of scoured bridge natural frequencies with soil–structure interaction. Soil Dynamics and Earthquake Engineering 2013;55:247–54. doi:10.1016/J.SOILDYN.2013.09.015.

[25] Prendergast LJ, Hester D, Gavin K, O'Sullivan JJ. An investigation of the changes in the natural frequency of a pile affected by scour. Journal of Sound and Vibration 2013;332:6685–702. doi:10.1016/J.JSV.2013.08.020.

[26] Malekjafarian, A., Kim, C. W., OBrien, E. J., Prendergast, L. J., Fitzgerald, P. C., & Nakajima, S. (2020). Experimental Demonstration of a Mode Shape-Based Scour-Monitoring Method for Multispan Bridges with Shallow Foundations. Journal of Bridge Engineering, 25(8), 04020050.

[27] Abaqus, V. (2014). 6.14 Documentation. Dassault Systemes Simulia Corporation, 651. 2014.

[28] Ragni L, Scozzese F, Gara F et al. Dynamic identification and collapse assessment of Rubbianello Bridge. In IABSE Symposium, Guimaraes 2019: Towards a Resilient Built Environment Risk and Asset Management - Report. pp. 619–626.

[29] Gazetas G. Formulas and Charts for Impedances of Surface and Embedded Foundations. Journal of Geotechnical Engineering 1991;117:1363–81. doi:10.1061/(ASCE)0733-9410(1991)117:9(1363).

[30] Carbonari S, Morici M, Dezi F, Leoni G. A lumped parameter model for time-domain inertial soil-structure interaction analysis of structures on pile foundations. Earthquake Engineering & Structural Dynamics 2018;47:2147–71. doi:10.1002/eqe.3060.

[31] Link O, García M, Pizarro A, Alcayaga H, Palma S. (2020). Local Scour and Sediment Deposition at Bridge Piers during Floods. *J Hydraul Eng*, *146*(3), 04020003.

[32] Scozzese, F., Tubaldi, E., & Dall'Asta, A. (2020). Assessment of the effectiveness of Multiple-Stripe Analysis by using a stochastic earthquake input model. Bulletin of Earthquake Engineering, 1-37.